JGR Space Physics

RESEARCH ARTICLE
10.1029/2024JA033003

Special Collection:
Space Weather Events of 2024 May 9-15

# Ionospheric Disturbances Observed Over the Peruvian Sector During the Mother's Day Storm (G5-Level) on 10–12 May 2024

**Ram Singh[1], Danny E. Scipión[1], Karim Kuyeng[1], Percy Condor[1], Cesar De La Jara[1], Juan Pablo Velasquez[1], Roberto Flores[1], and Edwar Ivan[1]**

[1]Radio Observatorio de Jicamarca, Instituto Geofísico del Perú, Lima, Peru

**Abstract** This article presents the recent extreme and rare G5-level geomagnetic storm (Mother's Day Storm) effects on the equatorial and low-latitude ionosphere observed at the Peruvian sector by the Jicamarca (11.9°S, 76.8°W, magnetic dip 1°N) incoherent scatter radar and associated instruments. This storm was produced by multiple Earth-directed coronal mass ejections, which generated significant modifications in the Earth's magnetic field, leading to the Sym-H of ∼−518 nT. On the dayside, due to the strong eastward penetration electric field, vertical plasma drift and equatorial electrojet (EEJ) enhanced for 2–3 hr and remained consistent at values of ∼95 m/s and 260 nT between 1700 and 1900 UT (1200 and 1400 LT). At the same time, vertical E × B plasma drift uplifted the equatorial ionosphere, producing the dusk-side super plasma fountain and transferring electron density to higher latitudes. A huge increase (∼1,325%) in electron density (from 11 to 142 TECu) is observed at low and mid-latitudes from ∼20°S to 50°S between 2000 and 0400 UT (1500–2300 LT). The strong westward penetration electric field suppressed pre-reversal enhancement, leading to downward plasma drift (∼−96 m/s) at around 2400 UT (1900 LT). Overnight, vertical plasma drift fluctuated between ±90 m/s, and the combined effect of penetration and disturbance dynamo electric fields caused a significant increase (∼530 km) in ionospheric virtual height. In the main and early recovery phase, consistent short- and long-duration electric field disturbances persisted for approximately 30 hr, with periods of ∼48 and 90 min.

**Key Points:**

- Strong eastward penetration electric field produced plasma fountain effect and poleward expansion of equatorial ionization anomaly crest
- Suppression of pre-reversal enhancement caused by strong westward penetration electric field
- Consistent oscillations in vertical plasma drift, EEJ, and IMF Bz

**Supporting Information:**

Supporting Information may be found in the online version of this article.

**Correspondence to:**

R. Singh,
ramphysics4@gmail.com

**Citation:**

Singh, R., Scipión, D. E., Kuyeng, K., Condor, P., De La Jara, C., Velasquez, J. P., et al. (2024). Ionospheric disturbances observed over the Peruvian sector during the Mother's Day Storm (G5-level) on 10–12 May 2024. *Journal of Geophysical Research: Space Physics*, *129*, e2024JA033003. https://doi.org/10.1029/2024JA033003

Received 25 JUN 2024
Accepted 5 NOV 2024

**Author Contributions:**

**Conceptualization:** Ram Singh, Danny E. Scipión, Karim Kuyeng, Juan Pablo Velasquez, Roberto Flores
**Data curation:** Ram Singh, Danny E. Scipión, Karim Kuyeng, Percy Condor, Cesar De La Jara, Juan Pablo Velasquez, Edwar Ivan
**Formal analysis:** Ram Singh, Danny E. Scipión, Karim Kuyeng, Cesar De La Jara, Roberto Flores, Edwar Ivan
**Funding acquisition:** Danny E. Scipión
**Investigation:** Ram Singh, Danny E. Scipión, Karim Kuyeng, Roberto Flores
**Methodology:** Ram Singh, Danny E. Scipión, Karim Kuyeng
**Project administration:** Danny E. Scipión



## 1. Introduction

On 10 and 11 May 2024, multiple enormous solar storms collided with the Earth's atmosphere, causing the most recent severe geomagnetic storm (G5-class). The previous geomagnetic storm of similar magnitude was observed in October 2003. For a geomagnetic storm to achieve its maximum intensity, coronal mass ejections (CMEs) must either merge or approach Earth around the same moment. This historically severe geomagnetic storm was initiated by several CMEs moving toward Earth. The primary cause of the CMEs was a big and complex sunspot cluster (NOAA area 3664), which was about 17 times the diameter of Earth and was the largest and most active sunspot in the current solar cycle 25. G5 storms are very rare, occurring on average every 11 years when a sunspot group develops, approximately one to three times the size of the Earth. A G5 geomagnetic storm may cause numerous and vast challenges with various power and communication systems, including voltage control problems, component failures in some power grid systems, signal blackouts, loss of GPS and other satellite navigation, and even human health (e.g., Doherty et al., 2004; Gaunt & Coetzee, 2007).

During the magnetic storm, significant modifications in the electrodynamics of the equatorial ionosphere can be disturbed due to the enhancement of magnetospheric convection, energy deposition through particle precipitation, Joule heating, and momentum at high latitudes (e.g., Kamide & Kokubun, 1996; Kikuchi et al., 1996; Tsurutani & Gonzalez, 1997). Electrodynamic changes can profoundly impact the distribution of plasma density, instability growth rate in the F region, and plasma drift motion in the equatorial and low-latitude ionosphere (e.g., Abdu, 2012; Fejer & Scherliess, 1997; Mannucci et al., 2005). Using the geomagnetic field, GPS TEC, ionosondes, and incoherent radar measurements, interplanetary electric field (IEF) penetration to the low latitude ionosphere has been comprehensively investigated (e.g., Fejer et al., 1979, 2021, 2024; Huang & Zhang, 2021; Rout et al., 2019, 2022; Singh et al., 2015, 2022). Using the Instituto Geofisico del Peru's (IGP) Jicamarca incoherent scatter radar measurements, Fejer et al. (2021, 2024) observed significant disturbances in vertical and zonal plasma drifts. They suggested that the upward and downward modifications are caused by under-shielding and over-shielding electric fields. Previous studies have shown a strong correlation between geomagnetic field,

**Resources:** Ram Singh, Danny E. Scipión, Karim Kuyeng, Percy Condor, Cesar De La Jara, Roberto Flores, Edwar Ivan
**Software:** Ram Singh, Danny E. Scipión, Karim Kuyeng, Percy Condor, Cesar De La Jara, Roberto Flores, Edwar Ivan
**Supervision:** Danny E. Scipión
**Validation:** Ram Singh, Danny E. Scipión, Karim Kuyeng, Percy Condor, Cesar De La Jara, Juan Pablo Velasquez, Edwar Ivan
**Visualization:** Ram Singh, Danny E. Scipión
**Writing – original draft:** Ram Singh, Danny E. Scipión
**Writing – review & editing:** Ram Singh, Danny E. Scipión, Karim Kuyeng, Percy Condor, Cesar De La Jara, Roberto Flores

ionospheric parameters perturbations at low latitude ionosphere, and interplanetary magnetic field (IMF) reorientation (e.g., Chakrabarty et al., 2015; Huang et al., 2005; Singh et al., 2022).

The sudden southward turning of the IMF's z-component (Bz) enhances magnetospheric plasma convection toward the Earth from the tail. The potential drop due to charge accumulation at the inner boundary of the ring current cancels out the effects of the primary magnetospheric convection electric field, known as prompt penetration (PP) or under shielding conditions (e.g., Chakrabarty et al., 2008; Huang et al., 2005; Kelley et al., 2003; Kikuchi et al., 1996). The PP electric field promptly enhanced the eastward and westward electric fields during the day and night, which can continually enhance the electric field close to the equator for minutes to hours (e.g., Huang et al., 2005; Kelley et al., 2003; Kikuchi et al., 1996).

Previous studies have shown large modifications in the F region plasma drifts caused by the polarity changes of IMF Bz (i.e., southward and northward) (e.g., Chakrabarty et al., 2015; Fejer et al., 2021, 2024; Huang & Zhang, 2021; Huang et al., 2005; Mannucci et al., 2005). Chakrabarty et al. (2015) showed continuous eastward electric perturbations and periodic oscillation triggered by the polarity changes of IMF Bz. The PP electric field can contribute to an increase in total electron content (TEC) at mid to higher latitudes due to the upliftment of the equatorial ionosphere by enhancement of E × B drift (e.g., Mannucci et al., 2005; Rout et al., 2019; Singh et al., 2022; Tsurutani et al., 2004). Mannucci et al. (2005) showed that the strong eastward PP electric field caused an increase in TEC (∼250% TECu) and poleward expansion of the equatorial ionization anomaly (EIA) crest.

The duration of the PP electric field is decided by the shielding and overshielding processes, as well as the penetration electric field's tendency to persist. The continuous and long-lasting durations of the PP electric field during the southern IMF Bz have been thoroughly examined (e.g., Kobea et al., 2000; Huang & Zhang, 2021; Huang et al., 2005). Huang and Zhang (2021) observed persistent perturbations in vertical plasma drift over Jicamarca for approximately 10 and 13 hr caused by the IEF condition. According to Huang et al. (2005), the electric field can penetrate the equatorial ionosphere for approximately 2 and 3 hr without sufficient shielding. Periodic polarity changes in the IMF Bz can penetrate the low-latitude ionosphere and cause periodic oscillations (e.g., Rout et al., 2022; Singh et al., 2022; Wei et al., 2008). Using the magnetometers, GPS TEC, and digisondes data from low to higher latitudes, Singh et al. (2022) showed ∼1-hr periodic oscillation of IEF penetration. Wei et al. (2008) showed that the penetration electric field oscillates periodically in the equatorial electric field, with periods ranging from 20 min to 3 hr.

Aside from the PP electric field, various additional factors (e.g., disturbance dynamo (DD) electric field, magnetospheric substorms, solar flares, and solar wind dynamic pressure) can contribute to causing disruptions in the equatorial and low latitude ionosphere (e.g., Blanc & Richmond, 1980; Chakrabarty et al., 2008; Huang & Zhang, 2021; Singh & Sripathi, 2017; Singh et al., 2015). During geomagnetic storm conditions, electric field interruption at lower latitudes with time delay produced by high latitude joule heating and global wind circulations is known as the DD electric field (e.g., Abdu et al., 2006). DD generates an opposite polarity electric field at low latitudes to the usual ionospheric dynamo electric field, during the day westward and eastward at night.

The main objective of the present study is to describe the ionospheric responses to the most severe (G5-class) geomagnetic storm over the equatorial and low-latitude ionosphere covering Peruvian longitudes. Our examination shows that the dusk-side super fountain effect is caused by a significant increase in vertical plasma drift ∼95 m/s in 150 km echoes and the F region. The continuance of the under-shielding electric field conditions produced the long-lasting PP electric field (lasting about 2 and 3 hr) at the equator. A strong westward PP electric field reduced the pre-reversal enhancement, resulting in a downward plasma drift of approximately −95 m/s and a decrease in virtual height by about 130 km. The combined effects of the PP and DD electric fields caused a significant increase (∼530 km) in the ionospheric virtual height, with the height exceeding 700 km, causing ionograms to go off-scale in Vertical Incidence Pulsed Ionospheric Radar (VIPIR). Continuous oscillations in the IMF Bz, equatorial electrojet (EEJ), and plasma drifts persisted for around 30 hr, with dominant periods of 48 and 90 min.

This work is presented in the following structure: Section 2 presents data sets and analysis. The observations and results are detailed in Section 3. Sections 4 and 5 give the discussion and conclusion, respectively.

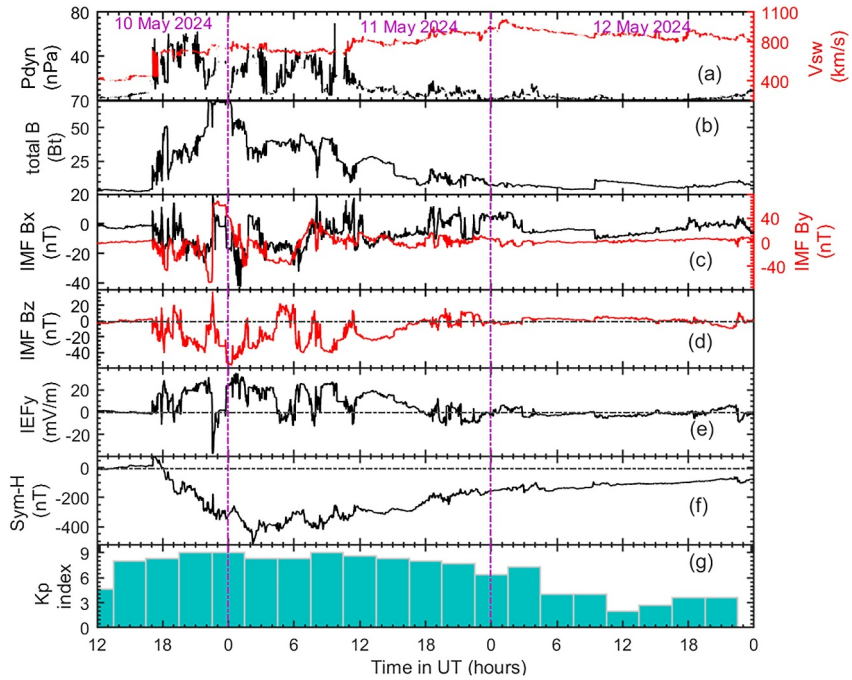


**Figure 1.** (a–f): Geomagnetic and interplanetary parameters for 10–12 May 2024. (a) Solar wind speed (Vsw) and solar wind dynamic pressure (Pdyn) in red and black curves; (b) total interplanetary magnetic field (Bt); (c) interplanetary magnetic field components (IMF) Bx (black) and Bx (red); (d) interplanetary electric field (IEFy); (e) Sym-H; and (f) Kp index.

## 2. Data Analysis

We evaluated multi-instrument data from the equatorial and low-latitude latitude ionosphere to examine the response to the Mother's Day magnetic storm. IGP's Jicamarca Unattended Long-term Investigations of the Ionosphere and Atmosphere Medium Power (JULIA MP) measurements for 150 km echoes (~120–200 km), F region plasma drifts, and plasma irregularities (small scale, 3-m), VIPIR for the virtual height (h'F), maximum frequency (foF2), and equatorial spread F (ESF), and the vertical total electron content (vTEC) from the global positioning system (GPS) receivers over the American longitudes are used. IGP's Jicamarca radar is the most effective radar for exploring the electrodynamics of the equatorial ionosphere and penetration electric field considering its geophysical location (11.9°S, 76.8°W, magnetic dip 1°N) and measurements. JULIA MP is a combined mode that uses two solid-state transmitters with a peak power of 96 kW to detect (a) coherent echoes such as equatorial electrojets, spread F, and 150 echoes and (b) incoherent echoes to estimate the zonal and vertical plasma drift of F region heights. The JULIA MP radar mode uses daytime ionospheric irregularities and Doppler-shifted echoes to estimate the zonal and vertical plasma drifts of around 150 km and F region. Detailed information on the IGP's Jicamarca radar measurements can be found in the following studies (e.g., Chau & Kudeki, 2013; Chau & Woodman, 2004; Fejer, 2011). The JULIA MP radar and ionosonde VIPIR recorded the ionospheric parameters at intervals of 5 and 7 min. The TEC data for the 30 s and 5-min time intervals is obtained from the MIT Haystack Observatory madrigal database (http://madrigal.haystack.mit.edu/madrigal/) and (ftp://cddis.gsfc.nasa.gov/pub/gps/data). The ground-based magnetometers at equatorial stations at Jicamarca (11.9°S, 76.8°W) and off equatorial station at Piura (5.2°S, 80.6°W) measured 1-min time resolution geomagnetic magnetic field variation. The difference between Jicamarca and Piura is used as a proxy for the strength of the equatorial electrojet (EEJ = $\Delta H_{Jic} - \Delta H_{piura}$). Geomagnetic (e.g., Kp index, Sym-H) and interplanetary solar wind (e.g., IMF B, solar wind speed, particle density) parameters are taken from Advance Composition Explorer (ACE) satellite measurements from the CDAWeb (https://cdaweb.gsfc.nasa.gov/).

## 3. Observation and Results

Figure 1 displays the interplanetary and geomagnetic conditions measured by the ACE spacecraft at the L1 point during the Mother's Day storm on 10–12 May 2024. The magnetic storm began around 1700 UT on May 10 and

ended at nearly 0300 UT on May 11, with a Sym-H value of approximately −518 nT. The recovery phase lasted more than a week, as the increased solar wind velocity provided additional momentum and energy to sustain it longer. The top panel of Figure (a) displays variations in solar wind velocity (Vsw) and solar wind dynamic pressure (Pdyn). Panels (b–e) illustrate variations in the interplanetary electric and magnetic fields (IMF and IEF), including (b) total magnetic field (Bt), (c) IMF Bx (blue), and IMF By (red), (d) IMF Bz and (e) IEF. The bottom two panels exhibit the geomagnetic indices Sym-H (a symmetric component of ring current) and Kp index. The Pdyn and Vsw experienced a sharp increase due to the arrival of an interplanetary shock, leading to a significant enhancement in sym-H, which rose by approximately +86 nT around 1730 UT on May 10. At the time of the interplanetary shock's arrival, Vsw, Pdyn, Bt, IEF, and Kp spiked from 450 to 750 km/s, 5 to 53 nPa, 2.5 to 45 nT, 4 to 28 mV/m, ∼10 to 86 nT, and 3 to 9, respectively. The magnetic field components exhibit continuous oscillations and large-magnitude variations, with a total magnitude change of around 72 nT (in Bt), 135 nT (in IMF By), 98 nT (in IMF Bz), and 65 mV/m (in IEF) between 2230 and 0000 UT on May 10 and 11. During the recovery phase, a maximum enhancement in the solar wind speed was recorded at ∼ 900 km/s at 1700 UT on May 11 and ∼1000 km/s at 1000 UT on May 12. The IMF Bz repeatedly showed consistent southward polarity between −30 and −50 nT over 2–7 hr, with additional polarity changes and irregular fluctuations throughout the main and early recovery phases. On May 10, IMF Bz fluctuated between 14 and −40 nT between 1700 and 1900 UT.

Significant variations were seen in the southerly direction for almost 3 hr, reaching a maximum of −50 nT between 1900 and 2200 UT. On May 10 and 11, significant polarity changes from south to north (−50 to 63 nT) occurred at 2200 UT, and then another southward change occurred and lasted around 6 hr between 2200 and 0400 UT. In Figure 1d, long-duration southward IMF Bz was noted between 1100 and 1800 UT on May 11. The IEF change has been calculated using the IMF Bz and the solar wind speed (−Vsw × Bz). Multiple substorms developed throughout the main and recovery phases, leading to substantial increases in the auroral electrojet index (SMU/SML) and Sym-H peaks, as illustrated in Figures S1 and S1d in Supporting Information S1. The SML index showed high activity (more than 3000 nT) between ∼1800–2000 UT and 0700–1600 UT on May 10–11.

Figure 2 presents IGP's Jicamarca radar measurements acquired between 1200 and 2100 UT (0700 and 1600 LT) on May 10, in the main phase of the magnetic storm. The top panel (a) shows incoherent echoes of the F region altitude from ∼200 to 600 km, (b) F region vertical plasma drift at different heights between 248 and 548 km, with an altitude interval of 60 km (cyan circles), and standard deviation (blue error bars). The green line plot indicates the average drift from the Scherliess and Fejer (SF) model (e.g., Scherliess & Fejer, 1999). Panel (c) displays the 150 km echoes and the vertical drift (black circle). The upward and downward plasma drift represents the eastward and westward electric fields in the equatorial ionosphere. During the day, the E region electron density peak to the bottom side F region ionosphere (particularly between 120 and 200 km) influences the entire ionosphere (e.g., Immel et al., 2018). Panel (d) depicts the virtual height (h'F) changes measured by the VIPIR over Jicamarca. Panel (e) exhibits the equatorial electrojet (EEJ, blue curve) and the five international quiet days (IQDs) average value (black line) for May. The EEJ is a proxy for the strength of ionospheric F region E × B vertical drift (e.g., Anderson et al., 2002). The bottom panel (e) shows IMF Bz variations. Significant changes in ionospheric parameters occurred at the same time between 1700 and 1900 UT (1200 and 1400 LT), as shown in Figure 2 (gray shaded area). The ionospheric parameters were initially quiet, and dramatic changes occurred when the IMF Bz turned sharply southward at around 1700 UT (1200 LT), resulting in the F region plasma drift, 150 km plasma drift, h'F, and EEJ to increase from 20 to 100 m/s, 20 to 100 m/s, 200 to 335 km, and 60 to 260 nT. After that, it progressively increased and remained stable for almost 2 hr, from 1700 to 1900 UT (1200–1400 LT). Surprisingly, the penetrating electric field persists for around 2 and 3 hr, leading to an upward plasma drift (eastward electric field) (e.g., Huang et al., 2005). The continuing penetration resulted in the dusk side super plasma fountain effect, where the equatorial ionization anomaly (EIA) crest extended poleward up to 20–50°S (in the southern hemisphere), and electron density increased ∼1,325%, as illustrated in Figures 3 and 4.

The latitude distribution of GPS total electron content (TEC) and EIA crest evolution in the Northern and Southern Hemispheres is shown in Figure 3. The upper and lower panels in the Figure (a–b and c–d) exhibit GPS TEC and deviation in TEC (dTEC) between −60 and 60°N latitudes (geographical latitude) over the American longitudes at ∼−77°E ± 10°E. The dTEC = (TEC − $TEC_{IQDs}$) measures the difference between the disturbed day's TEC and the five IQDs average TEC value. The EIA crest significantly increased and extended poleward to higher latitudes, as seen in Figures 3b and 3d. On May 10, TEC enhanced significantly ∼1,325% (∼130 TECu) in the southern hemisphere and ∼380% (∼115 TECu) in the northern hemisphere compared to the quiet days due to

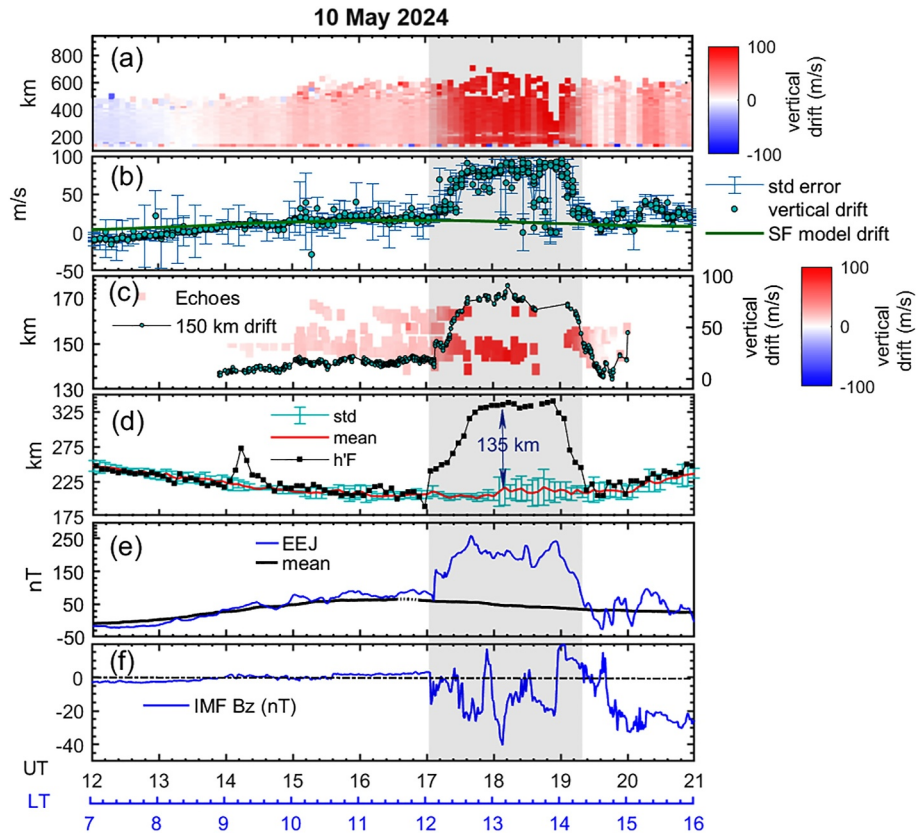


**Figure 2.** (a–f): Shows Jicamarca ISR observations from 1200 (0700) to 2100 (1600) UT (LT) on 10 and 11 May 2024. (a) F region vertical plasma drift from 200 to 945 km, (b) F region vertical drift at different altitudes (solid cyan circle); Scherliess and Fejer (SF) model average drift (green line plot) and standard deviation (blue error bars), (c) 150 km echoes and average drift (black circle), (d) equatorial electrojet (EEJ = $\Delta H_{Jic} - \Delta H_{piura}$) and international quiet days mean (IQDs) in blue and black curves, and (e) IMF Bz. The gray-shaded area indicates a dramatic increase in the ionospheric parameters.

the super plasma fountain effect (e.g., Mannucci et al., 2005; Tsurutani et al., 2004). Between 15°N to 38°N and 15°N to 50°S, the EIA crest strengthened significantly and expanded poleward. Significant increases in TEC occur on the dusk side for about 5 hr between 2000 and 0100 UT (1500–2000 LT) in the northern hemisphere and 1900–0400 UT (1500–2300 LT) for 7 hr in the southern hemisphere. The crest formation showed hemispheric deviations, with considerable increases in the southern hemisphere. The southern hemisphere experiences a greater increase in TEC and poleward expansion than the northern hemisphere due to strong eastward penetration and the seasonal anomaly (i.e., winter anomaly) effect (e.g., Tsurutani et al., 2004; Walker, 1981).

The GPS TEC variation and IQD mean values for low- and mid-latitude locations over American longitude for May 10 and 11 are shown in Figure 4. The top two panels (a and b) show TEC variation in the northern hemisphere at Santo Domingo (RDSD:18.4°N, 290.2°E) and Bogota (BOGT:4.6°N, 285.1°E), while the bottom panels (c and d) show TEC variation in the southern hemisphere at Cordoba (CORD:−31.5°N, 295.5°E) and Santiago (SANT:−33.1°N, 289.5°E). The red line plots in Figure 4 indicate individual pseudo-random noise (PRN) TEC variations, the blue line plots are the average value of all PRN TEC, and the black/gray lines represent the mean/standard deviation of five IQDs. Figure 4 shows large TEC improvements in the northern hemisphere from 1730 UT (1230 LT) to 0200 UT (2200 LT) which sustained around 8 hr. On May 10, a large TEC value increase at the RDSD and BOGT occurred at ∼380% TECu and 280% TECu, compared to the $IQD_S$ mean value at ∼2300 UT (1800 LT) and 2230 UT (1730 UT), respectively. In the southern hemisphere, TEC increased ∼1,150% and 1,325% at the CORD and SANT, respectively. The TEC increased drastically between 1730 UT (1230 LT) and 0730 UT (0230 LT) and lasted around 14 hr on May 10 and 11. This is the first time that we are seeing ∼1,325% TEC enhancements sustained for longer periods at low and mid-latitudes. This large growth in TEC at mid-

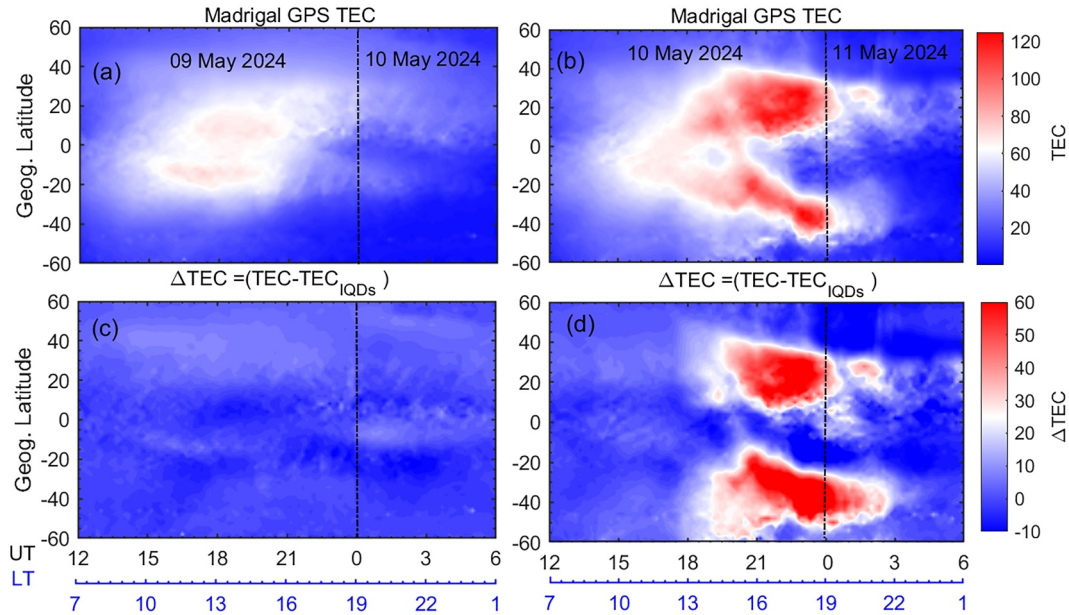


**Figure 3.** Panels (a and b) depict the latitudinal variations of madrigal GPS total electron content (TEC) over American longitudes at ∼−77°E ± 10°E on 09–11 May 2024. The bottom panels (c and d) represent ΔTEC = (TEC-TEC$_{IQDs}$ Mean), where TEC$_{IQDs}$ is the average value of five IQDs during May.

latitudes is due to the strong PP electric field effect, as persistent upward plasma drift and eastward EEJ (Figure 2) lead to dusk-side super plasma fountain.

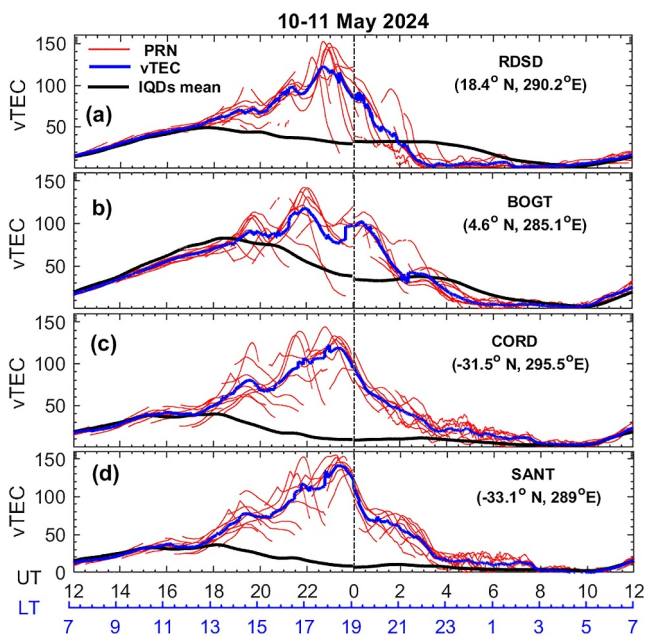


**Figure 4.** (a–d): Vertical TEC variations in the northern and southern hemispheres across the American longitudes (a) Santo Domingo (RDSD), (b) Bogota (BOGT), (c) Cordoba (CORD), and Santiago (SANT). The gray and blue curves symbolize the standard deviation and mean value of the five IQDs.

To examine ionospheric disturbances and plasma distributions associated with thermospheric neutral winds, we analyzed observations from two Fabry-Perot interferometers (FPI) measuring red line neutral winds at Millstone Hill (MH: 42.6°N, −72.5°W) and Cachoeira Paulista (CP: −22.7°S, 45.9°W) during the main and initial recovery phases of the magnetic storm (Figure 5). The meridional winds are displayed in the left panels (5a and 5c), while the right panels (5b and 5d) show the zonal winds at MH and CP. Positive and negative values of the meridional wind indicate northward and southward movement, respectively. For the zonal wind, positive values represent eastward flow, and negative values represent westward flow. The blue plots with error bars indicate the mean and standard deviation of the five IQDs for May. The wind variations on May 9 and 10 (green plots) serve as a control day to compare with disturbed day winds. At CP, a strong southward (negative) meridional wind of approximately −180 m/s developed in the southern hemisphere around 2200 UT (1900 LT). This wind weakened and gradually shifted northward (positive) around 0100 UT (2200 LT). Between 0100 and 0200 UT, a slow northward variation was observed at both MH and CP. The meridional component remained equatorward (southward) between 0200 UT (2100 LT) and 0500 UT (0000 LT), with a significant enhancement reaching about −280 m/s at MH. Around the same time, the meridional wind at CP also remained equatorward (northward) with values around +48 m/s.

On May 10 and 11, the zonal wind exhibited storm effects, leading to significant westward perturbations at both CP and MH. At CP, a strong westward zonal wind of −130 m/s developed, oscillated, and remained westward between 2200 and 0900 UT (1900 and 0600 LT) on May 10 and 11. At MH (Figure 5b), a strong westward zonal wind of approximately −182 m/s began at 0030 UT (1930 LT), weakened with oscillations, and remained westward

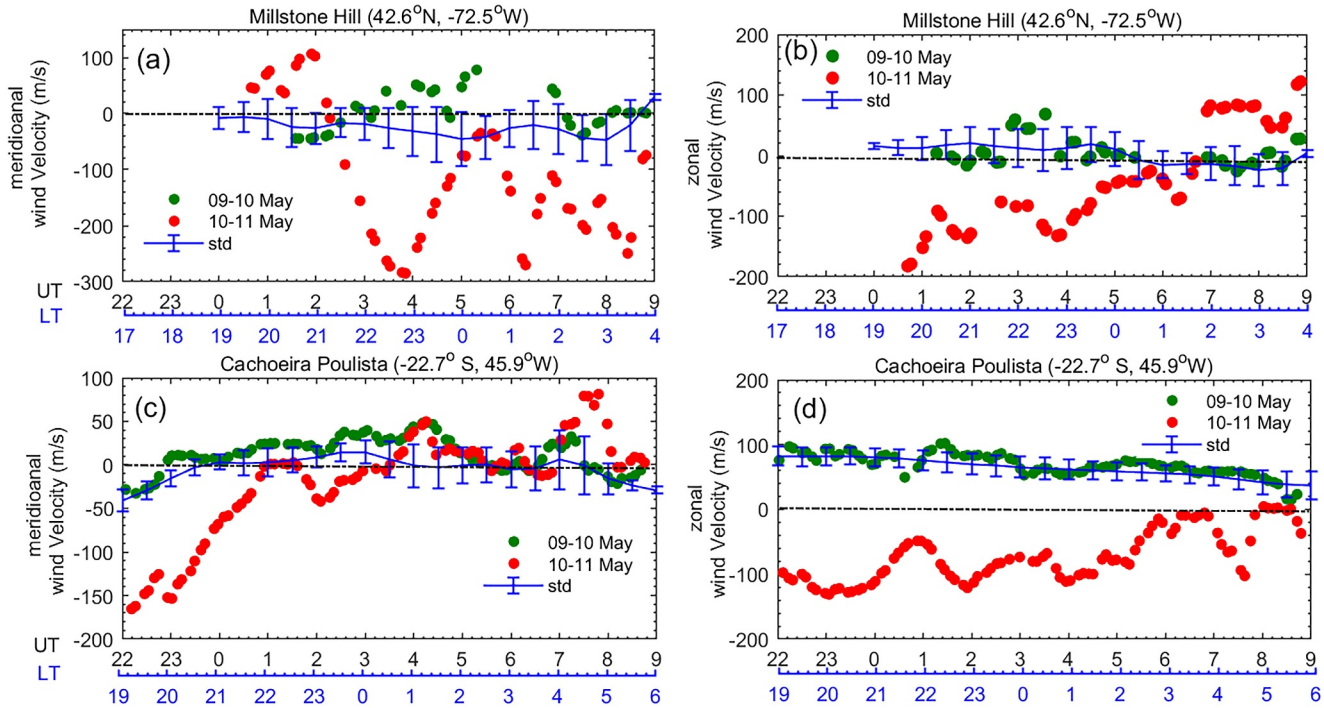


**Figure 5.** (a–d): Presents the FPI red line thermospheric neutral winds measured over Millstone Hill (panels a and b) and Cachoeira Paulista (panels c and d), along with the mean and standard deviation of the five IQDs. The left panels (a and c) display the meridional winds (positive values indicate northward winds, while negative values indicate southward winds), and the right panels (b and d) show the zonal winds (positive values represent eastward flow, while negative values represent westward flow).

until around 0530 UT (0030 LT). Significant changes in the meridional and zonal winds generate secondary ionospheric currents in the equatorial ionosphere, which can modify ionospheric plasma distribution (e.g., Abdu et al., 1998; Blanc & Richmond, 1980).

The coherent and incoherent backscatter power from equatorial spread F and plasma drift at various heights (between 248 and 548 km with 60 km height intervals), h'F, EEJ, and IMF Bz between 2100 and 1200 UT (1600–0700 UT) on May 10 and 11 shown in Figure 6. The green line plot indicates the climatological quiet time E × B drift variation. A strong, persistent westward penetrating electric field can be seen in Figures 6b and 6c between 2300 and 0030 UT (1800 and 1930 LT) that suppressed the pre-reversal enhancement. The westward penetration electric field lasted 1.5 hr, causing downward plasma (westward electric field) drift of around −90 m/s and ∼130 km reduction in h'F at ∼0000 UT (1900 LT), as represented by the shaded region in cyan. At the same time, IMF Bz and IEFy show large changes in their values, reaching approximately −58 nT and −35 mV/m, confirming the strong westward penetration electric field that produced the westward EEJ and downward plasma drift −40 nT and ∼−90 m/s at around. During the southward turning of IMF Bz, the F region plasma drift changed dramatically between 2300–0030 UT (1800–1930 LT), 0200–0300 UT (2300–0000 LT), 0600–0730 UT (0100–0230 LT), and 0800 UT (0300 LT). However, as the IMF Bz changed from south to north, the intensity of penetrations decreased due to overshielding electric field conditions. Following that, plasma drift increased/decreased in the upward/downward direction due to the northward/southward turning of IMF Bz at about 0030 UT (1930 LT). Upward plasma drift changes with high values of ∼90 m/s occurred for ∼3 hr between 0300 and 0600 UT (2200–0100 LT) matching with northward IMF Bz changes, indicated by the gray shaded area.

The most noticeable increase in virtual height occurred between 0300–0510 UT (2200–0010 LT) and 0730–0800 UT (0230–0300 LT), where the h'F increased approximately 530 km compared to the quiet day mean variation. Interestingly, the ionosphere uplifted to higher altitudes, and ionograms in the VIPIR went out of scale between 0530–0630 (0030–0130) and 0800–1030 (0300–0530) UT (LT), as seen by red lines in Figure 6d and Figure S2 in Supporting Information S1. In Figure 6a, the existence of large fluctuations in vertical drift between 0430 and 0830 UT (2330 and 0330 LT) which pushed up and down the small-scale (3-m) spread F irregularities. Initially,

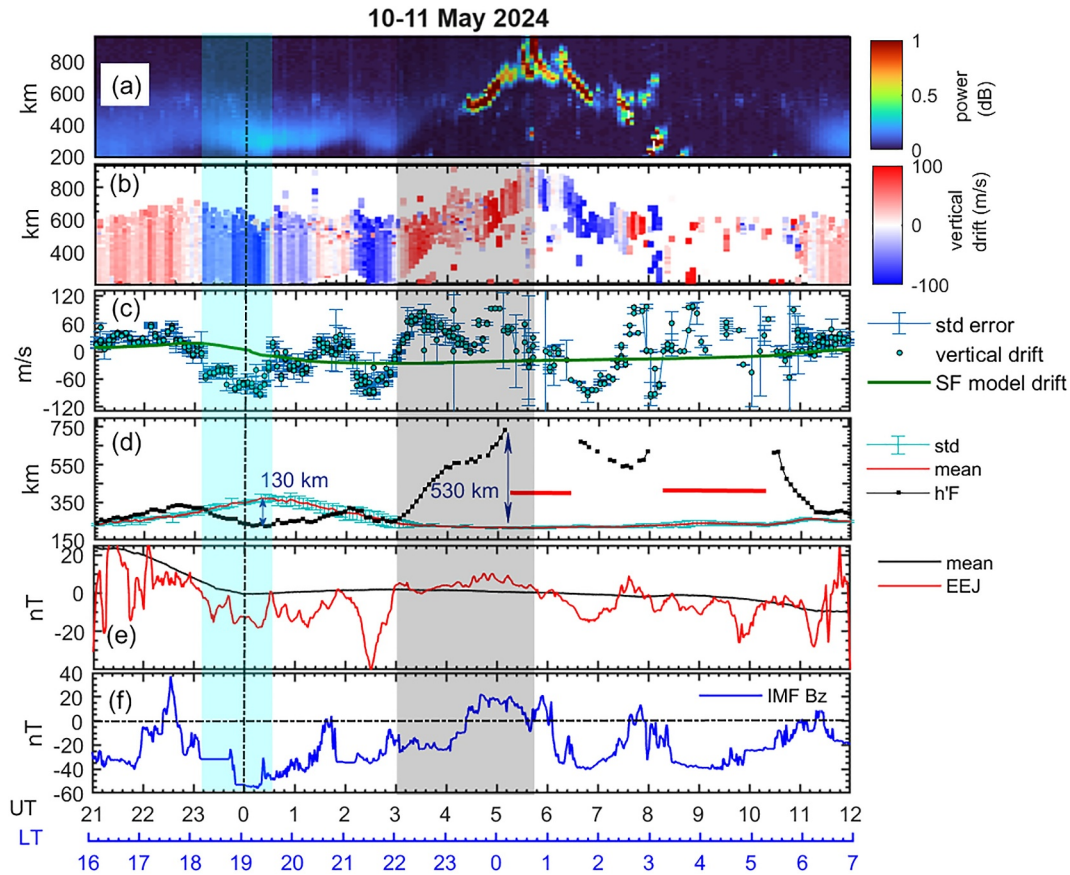


**Figure 6.** (a–f): Jicamarca ISR observations between 2100 (1600) and 1200 (0700) UT (LT) on 10 and 11 May 2024. (a) Coherent backscatter power from the equatorial spread F, (b) F-region vertical plasma drift, (c) F region vertical plasma drift (cyan solid circle) at different altitudes along with standard deviation (blue error bar) and SF model drift (green line), (d) h'F along with five IQDs mean, (e) EEJ (blue curve) with five IQDs average value (black line), and (f) IMF Bz. The blue and shaded areas represent significant downward and upward plasma drift enhancement.

spread F irregularities altitude was around 500 km, and the sudden increase in plasma drift (eastward electric field) with values ∼70 m/s pushed the irregularities to a higher altitude of ∼750 km at 0530 UT (0030 LT) then sudden downward plasma drift (westward electric field) dragged the irregularities at a lower altitude from ∼600 to 200 km at 0630 UT (0130 LT) and 0800 UT (0300 LT) with −70 m/s values. The equatorial ionosphere's electric field experiences disruptions during the night, oscillating periodically with periods of approximately 48 and 90 min (Figure 8). Both the disturbance dynamo-driven eastward electric field and the penetration electric field likely contributed to the observed increase in vertical plasma drift and h'F. These changes are likely due to significant alterations in thermospheric neutral winds (Figure 5), auroral electrojets (Figure S1 in Supporting Information S1), and the IMF Bz.

Variations in ionospheric parameters during the magnetic storm's recovery phase between 1000 and 1200 UT (0500 and 0700 LT) are shown in Figure 7. From top to bottom, panels indicate (a) vertical drifts from 200 to 800 km heights, (b) plasma drift at various heights (between 248 and 548 km with 60 km height intervals), (c) zonal drift (positive eastward and negative westward), (d) average zonal drift, (e) h'F, and (f) EEJ. The green and black curves in (b) and (f) indicate quiet time drift and IQDs mean variation. A maximum downward drift of approximately 50 m/s and a maximum westward drift of −180 m/s are shown in the Figure, which demonstrates the continuous downward (westward electric field) and westward zonal drift between 1100 and 1830 UT (0600 and 1330 LT). At the same time, the westward polarity electric field generates a counter electrojet (CEJ) or westward EEJ with values of ∼−245 nT, whereas the southward IMF Bz has a maximum negative value of −25 nT. Interestingly, the EEJ and zonal and vertical plasma drifts fluctuated with dominant periods of ∼90 min, as seen in gray shaded region. The vertical plasma drift and the strong westward EEJ changed remarkably

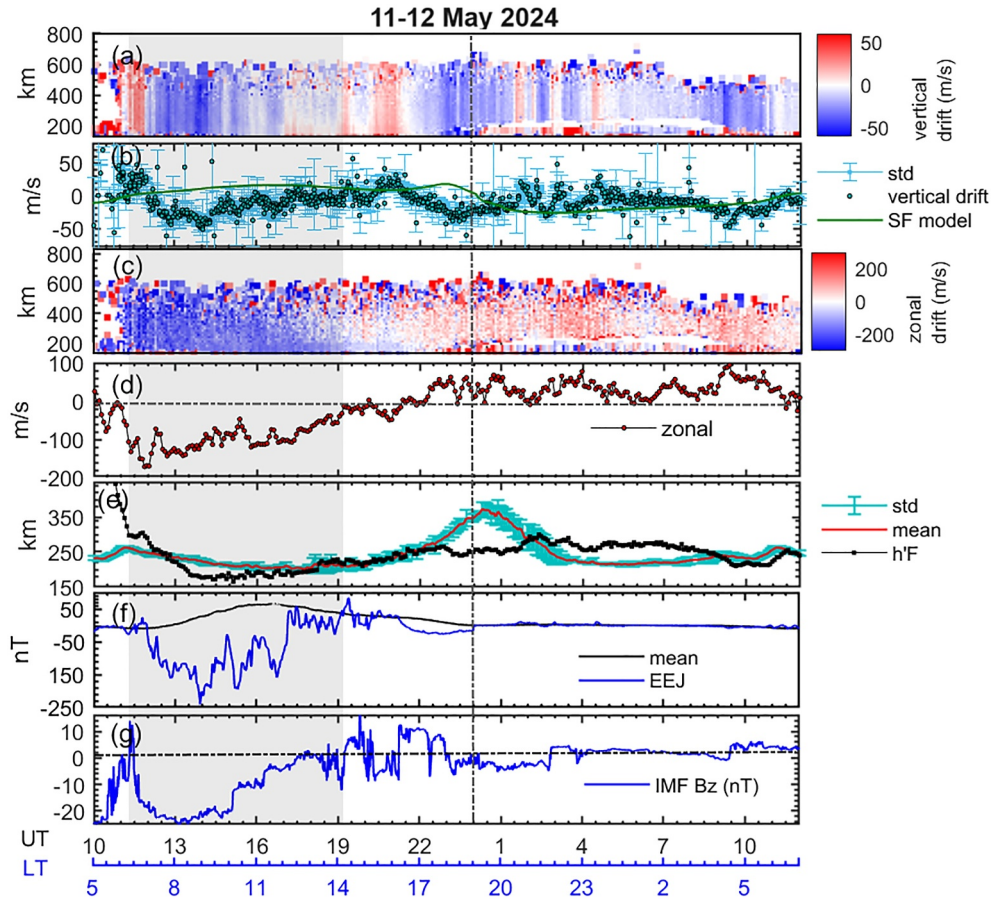


**Figure 7.** (a–g): Jicamarca ISR observations during 1000–1200 (0500–0700 LT) UT on 11 and 12 May 2024. (a) F-region vertical plasma drift (red solid circle) at various altitudes with standard deviation (blue error bar) and SF model drift (green line), (c) F region zonal drift, (d) average zonal drift, (e) h'F along with five IQDs mean, (f) EEJ (blue curve) and IQDs mean, and (g) IMF Bz. The gray shaded area represents the long-duration downward plasma drift and strong westward EEJ.

between 1130 and 1900 UT (0630 and 1400 LT), however, the zonal plasma drift remained westward or in the unmodified background direction. At the same time, IMF Bz shows similar variations, confirming the penetration electric field continues affecting the ionosphere for almost 8 hr (gray shaded area). Another long-duration westward electric field caused the downward plasma drift between 2000 and 2300 UT (1500–1800 LT) for about 3 hr, as westward EEJ and southward IMF Bz appeared.

As we noticed from our observations, vertical plasma drifts and EEJ are constantly fluctuating with IMF Bz. We performed a periodogram analysis applying the Lomb analysis in Figure 7. The Savitzky-Golay algorithm (e.g., Rout et al., 2022; Singh et al., 2022) is used to extract fast and short oscillations. In Figure 7, periodogram analysis carried out for the IMF Bz (green), EEJ (red), vertical plasma drift (cyan), and zonal drift (black) (a) between 1700 and 0300 UT (1200–2200 LT) from 10 to 12 May, (b) between 2100 and 1200 UT (1600–0700 LT) on 10 and 11 May, and (c) between 1000 and 0000 UT (0500–1900 LT) on 11 and 12 May. The IMF Bz, EEJ, and ionospheric drift experienced the same dominant continuous oscillations of ~48 and 90 min. The common and dominant periods evidence that the penetration electric field constantly disturbs the equatorial ionospheric electrodynamics.

## 4. Discussion

Using data from the IGP's Jicamarca Radio Observatory incoherent scatter radar, GPS TEC, VIPIR, and magnetometer, we examined ionospheric electrodynamic disturbances to the highest-level geomagnetic storm (G5) of the current solar cycle 25. The qualitative analysis reveals significant connections between IEF at low latitude ionospheric parameters (e.g., plasma drift, h'F, and EEJ) along the Peruvian longitudes. The equatorial

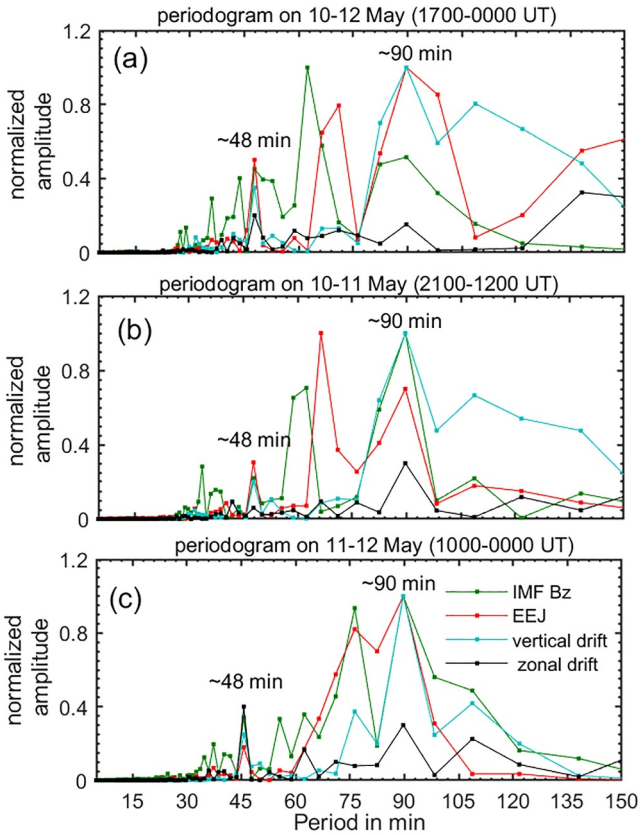


**Figure 8.** (a–c): Lomb-Scargle periodogram analysis for IMF Bz (green), EEJ (red), F region vertical plasma drift (cyan), and zonal plasma drift (black). The time range is selected from top to bottom panels: 1700–0000 UT on May 10–12, 2100–1200 on May 10–11, and 1000–0000 on May 11–12.

ionosphere heightened at higher altitudes with ∼95 m/s vertical plasma drift, causing the dusk-side plasma fountain and an increase in electron density of ∼1,325% at the low and mid-latitudes. The IMF, EEJ, and vertical plasma drift are all synchronized, demonstrating that under-shielding/over-shielding electric fields are continually disrupting the low-latitude ionosphere. The consistent disturbances in the zonal electric field at the equator lasted for approximately 2–3 hr and 8–10 hr. The sudden changes in the eastward electric field in the equatorial ionosphere caused by the penetration electric field have a noticeable impact on drifts, EEJ, and h'F. Interestingly, the arrival of an interplanetary shock, a sudden increase in solar wind dynamic pressure and velocity coincides with the northward to southward polarity change of the IMF Bz. This suggests that strong electric field disturbances are associated with both solar wind dynamic pressure and IMF Bz. The simultaneous sudden changes led to significant disturbances in the zonal electric field at the equator around 1730 UT (1230 LT). At this point, determining the individual effects is quite challenging.

The sharp southward (from northward) polarity changes in the IMF Bz increased the magnetospheric convection electric field and induced the under-shielding electric field condition, causing major changes in the equatorial zonal electric field (e.g., Chakrabarty et al., 2015; Fejer et al., 1979; Kelley et al., 2003). In the under-shielding state, IEF promptly maps to the equator via the propagation of a transverse magnetic mode in the Earth ionosphere waveguide, known as the prompt penetration (PP) electric field (e.g., Kikuchi et al., 1996). The PP electric field induced enhancements (eastward and westward) in the zonal electric field at the equator (during the day and night) (e.g., Chakrabarty et al., 2015; Fejer et al., 2021; Huang & Zhang, 2021). Our observations provide evidence that a strong persistent (approximate 2 and 3 hr) prompt penetration (PP) electric field increased vertical plasma drift (∼95 m/s) and eastward EEJ (∼260 nT) between 1200 and 1430 LT (1700 and 1930 UT) in Figure 2, resulting in a dusk side super plasma fountain effect (e.g., Tanaka & Ohtaka, 1996) and vertical TEC enhancements of more than ∼1,325% at low and mid-latitudes (Figures 3 and 4). As the interplanetary electric field gets stronger, the intensity of EEJ currents and E × B drift increases in eastward and upward direction, as observed by ground-based magnetometers and IGP's Jicamarca IS radar over the equator in Figure 2. Per our observations, a strong eastward penetration electric field constantly enhanced the pre-existing electric field at the equator and lifted the F region plasma at higher altitudes due to the E × B drift (e.g., Tsurutani et al., 2004; Mannucci et al., 2005; Huang et al., 2005; Rout et al., 2019).

Mannucci et al. (2005) reported a significant increase and poleward extension of the EIA peak during the Halloween storm of 29 and 30 October 2003. This was caused by the strong super-fountain effect and eastward PP electric field, which increased the F region electron density by about 250% at mid-latitudes. The recombination rate of the electron density contributes to how long the density remains. Electron density may last longer at higher altitudes due to slower recombination processes (Fuller-Rowell et al., 1996; Li et al., 2020). In our observations, electron density increased and remained stable until after sunset hours from 1900 to 0300 UT (1400–2200 LT), as shown in Figure 3. However, electron density at low latitude station SANT (Figure 4d) persisted for around 14 hr from 1730 to 0800 UT (1230–0300 LT) on 10 and 11 May.

On May 10, the poleward movement of meridional winds at CP between 2200 (1900) and 0030 (2130) UT (LT) (Figure 5c), combined with an existing eastward electric field (i.e., increased upward E × B drift) at the equator, contributed to the super plasma fountain effect and enhanced EIA peaks at higher latitudes. The weakening of the poleward winds began around 1900 LT and continued gradually until 2200 LT. Simultaneously, a strong westward penetration electric field restricted the upward movement of plasma during the pre-reversal enhancement, contributing to a reduction in the ionospheric virtual height due to downward plasma drift (Figures 6c and 6d) and initiating the onset of the CEJ condition (Figure 6e). Consequently, plasma accumulates at lower altitudes in the F-region, where the recombination rate is faster, leading to an increase in TEC, as shown in

Figure 4 between 1800 and 2130 LT. While recombination occurs more rapidly at lower altitudes due to increased neutral density, the westward electric field and suppression of the PRE contribute to a downward plasma drift in the F-region. This downward drift confines plasma to lower altitudes, where it accumulates. Although recombination rates are higher at these altitudes, the overall plasma loss does not occur instantaneously. As a result, the downward drift leads to significant plasma accumulation at these altitudes, causing an increase in TEC. Additionally, during the night, the cooling ionosphere reduces recombination rates, allowing the elevated plasma density to persist, particularly under the influence of electric fields that restrict upward plasma drift. The considerable increases in TEC at dusk and night can also be connected to the strong eastward penetration electric field that occurs just before dusk between 1200 and 1430 LT, as demonstrated in Figure 2. This enhanced eastward electric field generates upward E × B drift, which drives the ionospheric plasma to higher altitudes in the F-region, where the plasma experiences a slower recombination rate, allowing it to persist longer and contribute to sustained TEC levels. As dusk approaches, the ionization generated during the day accumulates in the ionosphere, and the gradual decay of solar radiation does not deplete the plasma quickly. This leads to an increase in TEC. Moreover, the significant enhancement of TEC at dusk and night is influenced not only by ionospheric processes, such as pre-reversal enhancement and slower recombination but also by plasmaspheric erosion. This process provides additional plasma to the ionosphere, as plasma stripped from the plasmasphere migrates downward and merges with the ionospheric plasma, keeping TEC values high. During a geomagnetic storm, the plasma fountain effect, and density enhancements at low and midlatitudes can be impacted by plasmasphere erosion (e.g., Chen & Schulz, 2001; Foster et al., 2002). The erosion caused by the strong convection electric field reduces the plasmasphere's total plasma density, transporting plasma into the ionosphere, especially at night in places far from the equator (e.g., Foster et al., 2002). According to our findings, the increase in electron density observed in the southern hemisphere at night (Figures 3 and 4) could be attributed to plasmasphere erosion.

Studies using observational data as well as numerical models have investigated constant (approximately 2 and 3 hr) IEF penetration into the low-latitude ionosphere (e.g., Huang et al., 2005; Huba et al., 2005; Maruyama et al., 2007). The penetration electric field durations of about 2–3 and 1.5 hr in the vertical plasma flow are shown in Figures 2 and 5. Our observations in Figure 5 demonstrated that a strong westward penetration electric field caused reduction in pre-reversal enhancement and downward plasma drift (−95 m/s) at ∼00 UT (1900 LT), while an over-shielding electric field prompted an increase in upward plasma drift (∼60 m/s) at 0030 UT (1930 LT) (e.g., Chakrabarty et al., 2015; Fejer et al., 2021; Singh & Sripathi, 2017, 2021). Singh and Sripathi (2017) showed a large decrease in the pre-reversal enhancement over Indian longitudes due to the strong westward penetrating electric field, where the F region height was reduced significantly.

In our analysis, the causal relationship between the vertical plasma drift and the IEF suggested that the PP electric field caused continuous disturbances in the electrodynamics of the ionosphere for about 35 hr. The duration of the penetration electric field is controlled by the shielding and over-shielding state processes. Previous studies have shown that the rapid penetration electric field can exist for a longer period and play a major role in triggering the development of low-latitude ionospheric disturbances (e.g., Huang et al., 2005; Kobea et al., 2000; Wei et al., 2008). Wei et al. (2008) found a significant correlation (∼0.71) between IEF and zonal electric field over the Peruvian sector, with continuous penetration for ∼125 hr.

On 10 and 11 May, thermospheric neutral winds (meridional and zonal) at both MH and CP (Figure 5) exhibited substantial westward and equator deviations compared to quiet-time mean variation. These pronounced changes in the westward and meridional winds indicate large-scale disturbances in the neutral winds and ionospheric dynamo (e.g., Blanc & Richmond, 1980; Fejer & Scherliess, 1997). During the nighttime hours on May 10 and 11, a strong eastward DD electric field was generated due to strong westward zonal winds, leading to oscillations and a substantial increase in ionospheric virtual height, as shown in Figure 6. Since substantial modifications occurred concurrently in the IMF Bz, substorms (Figure S1 in Supporting Information S1), and thermospheric neutral winds (Figure 5), the combined effect of the ionospheric DD and penetration electric fields enhanced the ionospheric virtual height (Figure 6d) and oscillations in vertical plasma drift (Figure 6c).

On May 11, the downward vertical plasma drift resulted from an uninterrupted westward penetration electric field that continued for approximately 8–10 hr between 1100 and 2100 UT (0600 and 1600 LT) under the southward IMF Bz condition, as shown in Figure 7. The downward F region plasma drift and oscillations during the ongoing westward electric field (Figure 7) are very similar to the IEF variations, and the background zonal plasma drift velocity direction remains unchanged, which suggests that the IEF along with ionospheric dynamo consistently

induces the strong westward electric field. Huang et al. (2005) reported a considerably longer duration (~8–10 hr) of penetration electric field under the long-period IMF Bz. They suggested that the IEF can continually penetrate the low-latitude ionosphere without effective shielding under increased geomagnetic activity. According to Maruyama et al. (2005), storm-time perturbations in the zonal electric field are primarily generated by the PP electric field during the day. However, at night, the magnitudes of the DD electric field and PP electric field are nearly comparable. In this study, ionospheric electric field disturbances during the afternoon and PRE periods are linked to the PP penetration electric field, as the zonal electric field responds progressively to PP influences (e.g., Abdu et al., 1998). On the other hand, perturbations in ionospheric plasma drift at night may be induced by a combination of DD and PP electric fields. It is challenging to differentiate the distinct impacts of the DD and PP electric field effects when the IMF Bz, disturbance winds, and substorms occur simultaneously.

The polarity of the IMF leads the plasma to move up and down, resulting in an increase and decrease in E × B drift, which reacts similarly to EEJ intensity. The EEJ enhancement in the opposite direction (i.e., westward) is known as the equatorial counter electrojet (CEJ). The intensity of the electrojet modified the F region plasma drift, h'F, foF2, and TEC (e.g., Fejer et al., 2021; Kobea et al., 2000; Singh & Sripathi, 2021). Kobea et al. (2000) showed that long-duration overshielding (~3 hr) increased the intensity of equatorial electrojets in the westward direction (i.e., CEJ). Our measurements on May 11 between 0600 and 1600 LT (1100 and 2100 UT) under the strongly southward IMF Bz condition show an enhancement in CEJ (~−240 nT) associated with the long-duration continuous westward electric field (~6–8 hr), as shown in Figure 7 by gray shaded region.

The oscillation in F region plasma drifts and electrojets are presumably induced by the IEF's continuous penetration into the low latitude ionosphere throughout the main and early recovery phase of the magnetic storm. Wei et al. (2008) proposed that the periodic oscillation in the IMF Bz can continuously penetrate the low-latitude ionosphere and remain active for as long as the IMF Bz oscillates between north and south directions, which might be longer duration. Magnetospheric substorms with eastward and westward polarity on the dayside and nightside may also initiate the PP electric field at low latitudes under constant southward IMF Bz conditions (e.g., Chakrabarty et al., 2008; Fejer et al., 2021; Huang & Zhang, 2021). According to our observations, IMF Bz is not stable and oscillates, and influential substorms also occur. As a result, PP electric field triggered oscillations in EEJ and F-region drifts on the day and night side might be attributed to a combination of IMF Bz fluctuations and multiple substorms. The repetitive electric field disturbances cause quasi-periodic oscillations in IMF Bz, EEJ, and plasma drifts, with dominating periods ranging from 48 to 90 min, as shown in Figure 8.

## 5. Conclusion

We investigated the ionospheric responses to the most powerful geomagnetic storm of the current solar cycle 25, with Sym-H reaching approximately −518 nT. Throughout the magnetic storm, the IMF Bz oscillated and triggered long and short periods under shielding and overshielding electric field conditions. Using the IGP's Jicamarca radar and other supporting instruments, we examined the following important results:

1. The long-duration penetration electric field intensified vertical plasma drift, leading to the dusk side super plasma fountain phenomenon. The long-duration penetration electric field transpired when the IMF Bz remained stable in the southward direction.
2. On May 10, the significant eastward penetration electric field increased the eastward EEJ reaching ~260 nT on the dayside. On May 11, the long-duration strong westward electric field manifested in a westward EEJ ~−240 nT.
3. The equatorial ionization anomaly (EIA) increased and extended to mid-latitudes (15–38°N in the northern hemisphere, 20–50°S in the southern hemisphere).
4. Total electron content (TEC) increased ~1,325% and 380% in the southern and northern hemispheres, lasting 8–14 hr, and persevered till 2300 LT over the American longitudes.
5. The strong westward penetration electric field reduced pre-reversal enhancements, leading to downward plasma drift and CEJ ~−90 m/s and −40 nT, which corresponds with southward IMF Bz ~58 nT (IEFy ~35 mV/m).
6. During the local nighttime hours, the ionosphere reached higher altitudes due to the enhanced eastward electric field, and ionograms reached out of the range in VIPIR.
7. The IMF Bz, EEJ, and vertical plasma drift reflect the common and dominating period of ~48–90 min, which lasts around 30 hr in response to the ongoing penetrating electric field.

We conclude that the strong eastward PP electric field effect is responsible for the simultaneous sudden rises in the EEJ, 150 km drift, vertical plasma drift, and h'F during the storm's main phase. The strong eastward PP electric field produced dusk-side plasma fountain and large enhancements in vTEC from low to higher latitudes. The strong westward PP electric field suppressed the pre-reversal enhancement. At the same time, consistent (approximately 2 and 3 hr constant) shifts in IMF Bz, EEJ, and vertical plasma drift confirm continuous PP electric field condition. The common and dominating periods (~48 and 90 min) of IMF Bz, EEJ, and plasma drifts establish the causal association between IMF and ionospheric electrodynamics.

## Data Availability Statement

Interplanetary solar wind and geomagnetic data are sourced from the https://cdaweb.gsfc.nasa.gov/. Neutral winds and GPS TEC data are obtained from the MIT Haystack madrigal database (http://madrigal.haystack.mit.edu/madrigal/) and the worldwide TEC data sets from Crustal Dynamics Data Information System (CDDIS) (ftp://cddis.gsfc.nasa.gov/pub/gps/data). Magnetometer and VIPIR data provided by the Low-Latitude Ionospheric Sensor Network (LISN) (http://lisn.igp.gob.pe/). Vertical and zonal plasma drift data have been obtained from the Jicamarca madrigal database (https://www.igp.gob.pe/observatorios/radio-observatorio-jicamarca/madrigal/list). For more details on IGP ISR data, Danny E. Scipion (dscipion@igp.gob.pe) can be contacted.

**Acknowledgments**
This work is carried out at the Jicamarca Radio Observatory, Lima Peru. The Jicamarca Radio Observatory is a facility of the Instituto Geofísico del Perú operated through an agreement with Cornell University, under Prime Agreement AGS-2213849 from the National Science Foundation. We thank NASA/GSFC for permitting us access to the OMNIWeb (CDAWeb) service and the OMNI data used in this study. We also thank the GPS-TEC data provided by the Madrigal database and the online archives of the Crustal Dynamics Data Information System (CDDIS) of the NASA Goddard Space Flight Canter. We express our thanks to the Low-Latitude Ionospheric Sensor Network (LISN) for the magnetometers and VIPIR data. The LISN is funded by NSF Grant AGS-1933056 and a project led by the University of Texas Dallas in collaboration with the Instituto Geofísico del Perú and other institutions that provide information in the benefit of the space weather scientific community.

## References

Abdu, M. A. (2012). Equatorial spread F/plasma bubble irregularities under storm time disturbance electric fields. *Journal of Atmospheric and Solar-Terrestrial Physics*, *75–76*, 44–56. https://doi.org/10.1016/j.jastp.2011.04.024

Abdu, M. A., De Souza, J. R., Sobral, J. H. A., & Batista, I. S. (2006). Magnetic storm associated disturbance dynamo effects in the low and equatorial latitude ionosphere. In B. Tsurutani, R. McPherron, G. Lu, J. H. A. Sobral, & N. Gopalswamy (Eds.), *Recurrent magnetic storms: Corotating solar wind streams*. AGU. https://doi.org/10.1029/167GM22

Abdu, M. A., Sastri, J. H., Luhr, H., Tachihara, H., Kitamura, T., Trivedi, N. B., & Sobral, J. H. A. (1998). DP 2 electric field fluctuations in the dusktime dip equatorial ionosphere. *Geophysical Research Letters*, *25*(9), 1511–1514. https://doi.org/10.1029/98gl01096

Anderson, D., Anghel, A., Yumoto, K., & Kudeki, E. (2002). Estimating daytime vertical E × B drift velocities in the equatorial F region using ground-based magnetometer observations. *Geophysical Research Letters*, *29*(12), 1596. https://doi.org/10.1029/2001GL014562

Blanc, M., & Richmond, A. D. (1980). The ionospheric disturbance dynamo. *Journal of Geophysical Research*, *85*(A4), 1669–1686. https://doi.org/10.1029/ja085ia04p01669

Chakrabarty, D., Rout, D., Sekar, R., Narayanan, R., Reeves, G. D., Pant, T. K., et al. (2015). Three different types of electric field disturbances affecting the equatorial ionosphere during a long-duration prompt penetration event. *Journal of Geophysical Research: Space Physics*, *120*(6), 4993–5008. https://doi.org/10.1002/2014JA020759

Chakrabarty, D., Sekar, R., Sastri, J. H., & Ravindran, S. (2008). Distinctive effects of interplanetary electric field and substorm on nighttime equatorial F layer: A case study. *Geophysical Research Letters*, *35*(19). https://doi.org/10.1029/2008GL035415

Chau, J. L., & Kudeki, E. (2013). Discovery of two distinct types of 150 km radar echoes. *Geophysical Research Letters*, *40*, 4509–5414. https://doi.org/10.1002/grl.50893

Chau, J. L., & Woodman, R. F. (2004). Daytime vertical and zonal velocities from 150 km echoes: Their relevance to F region dynamics. *Geophysical Research Letters*, *31*(17), L17801. https://doi.org/10.1029/2004GL020800

Chen, M. W., & Schulz, M. (2001). Simulations of plasmaspheric plume formation during the magnetic storm of 21–23 April 2001. *Geophysical Research Letters*, *28*(1), 115–118. https://doi.org/10.1029/2000GL012554

Doherty, P., Coster, A. J., & Murtagh, W. (2004). Space weather effects of October–November 2003. *GPS Solutions*, *8*(4), 267–271. https://doi.org/10.1007/s10291-004-0109-3

Fejer, B. G. (2011). Low latitude ionospheric electrodynamics. *Space Science Reviews*, *158*(1), 145–166. https://doi.org/10.1007/s11214-010-9690-7

Fejer, B. G., Gonzales, C. A., Farley, D. T., Kelley, M. C., & Woodman, R. F. (1979). Equatorial electric fields during magnetically disturbed conditions 1. The effect of the interplanetary magnetic field. *Journal of Geophysical Research*, *84*(A10), 5797–5802. https://doi.org/10.1029/JA084iA10p05797

Fejer, B. G., Laranja, S. R., & Condor, P. (2024). Multi-process driven unusually large equatorial perturbation electric fields during the April 2023 geomagnetic storm. *Frontiers in Astronomy and Space Sciences*, *11*, 1351735. https://doi.org/10.3389/fspas.2024.1351735

Fejer, B. G., Navarro, L. A., Sazykin, S., Newheart, A., Milla, M., & Condor, P. (2021). Prompt penetration and substorm effects over Jicamarca during the September 2017 geomagnetic storm. *Journal of Geophysical Research: Space Physics*, *126*(8), 1–11. https://doi.org/10.1029/2021JA029651

Fejer, B. G., & Scherliess, L. (1997). Emperical models of storm time equatorial zonal electric fields. *Journal of Geophysical Research*, *102*(A11), 24047–24056. https://doi.org/10.1029/97ja02164

Foster, J. C., Erickson, P. J., Goldstein, J., & Rich, F. J. (2002). Ionospheric signatures of plasmaspheric tail erosion. *Geophysical Research Letters*, *29*(13). https://doi.org/10.1029/2002GL015067

Fuller-Rowell, T. J., Codrescu, M. V., Rishbeth, H., Moffett, R. J., & Quegan, S. (1996). On the seasonal response of the thermosphere and ionosphere to geomagnetic storms. *Journal of Geophysical Research*, *101*(A2), 2343–2353. https://doi.org/10.1029/95ja01614

Gaunt, C. T., & Coetzee, G. (2007). Transformer failures in regions incorrectly considered to have low GIC risk. In *IEEE Lausanne Power Tech* (pp. 807–812).

Huang, C.-S., Foster, J. C., & Kelley, M. C. (2005). Long-duration penetration of the interplanetary electric field to the low-latitude ionosphere during the main phase of magnetic storms. *Journal of Geophysical Research*, *110*(A11), A11309. https://doi.org/10.1029/2005JA011202

Huang, C.-S., & Zhang, Y. (2021). Equatorial plasma drifts during the magnetic storm on November 7–11, 2004: Identifications of the roles of penetration and disturbance dynamo electric fields with multi-instrumental measurements. *Journal of Geophysical Research: Space Physics*, *126*(9), e2021JA029386. https://doi.org/10.1029/2021ja029386

Huba, J. D., Joyce, G., Sazykin, S., Wolf, R., & Spiro, R. (2005). Simulation study of penetration electric field effects on the low- to mid-latitude ionosphere. *Geophysical Research Letters*, *32*(23), L23101. https://doi.org/10.1029/2005GL024162

Immel, T. J., England, S. L., Mende, S. B., Heelis, R. A., Englert, C. R., Edelstein, J., et al. (2018). The ionospheric connection explorer mission: Mission goals and design. *Space Science Reviews*, *214*(1), 13–36. https://doi.org/10.1007/s11214-017-0449-2

Kamide, Y., & Kokubun, S. (1996). Two-component auroral electrojet: Importance for substorm studies. *Journal of Geophysical Research*, *101*(A6), 13027–13046. https://doi.org/10.1029/96ja00142

Kelley, M. C., Makela, J. J., Chau, J. L., & Nicolls, M. J. (2003). Penetration of the solar wind electric field into the magnetosphere/ionosphere system. *Geophysical Research Letters*, *30*(4), 1158. https://doi.org/10.1029/2002GL016321

Kikuchi, T., Luhr, H., Kitamura, T., Saka, O., & Schlegel, K. (1996). Direct penetration of the polar electric field to the equator during a DP 2 events detected by the auroral and equatorial magnetometer chains and the EISCAT radar. *Journal of Geophysical Research*, *101*(A8), 17161–17173. https://doi.org/10.1029/96ja01299

Kobea, A. T., Richmond, A. D., Emery, B. A., Peymirat, C., Luhr, H., Morretto, T., et al. (2000). Electro-dynamic coupling of high and low latitudes: Observations on May 27, 1993. *Journal of Geophysical Research*, *105*(A10), 22979–22989. https://doi.org/10.1029/2000ja000058

Li, Q., Huang, F., Zhong, J., Zhang, R., Kuai, J., Lei, J., et al. (2020). Persistence of the long-duration daytime TEC enhancements at different longitudinal sectors during the August 2018 geomagnetic storm. *Journal of Geophysical Research: Space Physics*, *125*(11), e2020JA028238. https://doi.org/10.1029/2020ja028238

Mannucci, A. J., Tsurutani, B. T., Iijima, B. A., Komjathy, A., Saito, A., Gonzalez, W. D., et al. (2005). Dayside global ionospheric response to the major interplanetary events of October 29–30, 2003 "Halloween Storms". *Geophysical Research Letters*, *32*(12), L12S02. https://doi.org/10.1029/2004GL021467

Maruyama, N., Richmond, A. D., Fuller-Rowell, T. J., Codrescu, M. V., Sazykin, S., Toffoletto, F. R., et al. (2005). Interaction between direct penetration and disturbance dynamo electric fields in the storm-time equatorial ionosphere. *Geophysical Research Letters*, *32*(17), L17105. https://doi.org/10.1029/2005GL023763

Maruyama, N., Sazykin, S., Spiro, R. W., Anderson, D., Anghel, A., Wolf, R. A., et al. (2007). Modeling storm-time electrodynamics of the low-latitude ionosphere thermosphere system: Can long-lasting disturbance electric fields be accounted for? *Journal of Atmospheric and Solar-Terrestrial Physics*, *69*(10– 11), 1182–1199. https://doi.org/10.1016/j.jastp.2006.08.020

Rout, D., Pandey, K., Chakrabarty, D., Sekar, R., & Lu, X. (2019). Significant electric field perturbations in low latitude ionosphere due to the passage of two consecutive ICMEs during 6–8 September 2017. *Journal of Geophysical Research: Space Physics*, *124*(11), 9494–9510. https://doi.org/10.1029/2019ja027133

Rout, D., Singh, R., Pandey, K., Pant, T., Stolle, C., Chakrabarty, D., et al. (2022). Evidence for the presence of a global quasi-resonant mode of oscillations during High-Intensity Long-Duration Continuous AE Activity (HILDCAA) events. *Earth Planets and Space*, *74*(1), 91. https://doi.org/10.1186/s40623-022-01642-1

Scherliess, L., & Fejer, B. G. (1999). Radar and satellite global equatorial F region vertical drift model. *Journal of Geophysical Research*, *104*(A4), 6829–6842. https://doi.org/10.1029/1999ja900025

Singh, R., Lee, Y. S., Song, S. M., Kim, Y. H., Yun, J. Y., Sripathi, S., & Rajesh, B. (2022). Ionospheric density oscillations associated with recurrent prompt penetration electric fields during the space weather event of 4 November 2021 over the East-Asian sector. *Journal of Geophysical Research: Space Physics*, *127*(6), e2022JA030456. https://doi.org/10.1029/2022JA030456

Singh, R., & Sripathi, S. (2017). Ionospheric response to 22–23 June 2015 storm as investigated using ground-based ionosondes and GPS receivers over India. *Journal of Geophysical Research: Space Physics*, *122*(11), 11645–11664. https://doi.org/10.1002/2017ja024460

Singh, R., & Sripathi, S. (2021). The role of storm-time electrodynamics in the dawn and dusk sectors across equatorial and low-latitude ionosphere during December 19–21, 2015. *Journal of Geophysical Research: Space Physics*, *126*(8), e2020JA029072. https://doi.org/10.1029/2020ja029072

Singh, R., Sripathi, S., Sreekumar, S., Banola, S., Emperumal, K., Tiwari, P., & Kumar, B. S. (2015). Low-latitude ionosphere response to super geomagnetic storm of 17/18 March 2015: Results from a chain of ground-based observations over Indian sector. *Journal of Geophysical Research: Space Physics*, *120*(12), 10864–10882. https://doi.org/10.1002/2015ja021509

Tanaka, T., & Ohtaka, K. (1996). Ionospheric disturbances during low latitude auroral events and their association with magnetospheric processes. *Journal of Geophysical Research*, *101*(A8), 17151–17159. https://doi.org/10.1029/96ja00832

Tsurutani, B. T., & Gonzalez, W. D. (1997). The interplanetary causes of magnetic storms: A review. In B. T. Tsurutani, W. D. Gonzalez, Y. Kamide, & J. K. Arballo (Eds.), *Magnetic storms*.

Tsurutani, B. T., Mannucci, A., Iijima, B., Abdu, M. A., Sobral, J. H. A., Gonzalez, W., et al. (2004). Global dayside ionospheric uplift and enhancement associated with interplanetary electric fields. *Journal of Geophysical Research*, *109*(A8), A08302. https://doi.org/10.1029/2003ja010342

Walker, G. O. (1981). Longitudinal structure of the F-region equatorial anomaly—A review. *Journal of Atmospheric and Terrestrial Physics*, *43*(8), 763–774. https://doi.org/10.1016/0021-9169(81)90052-0

Wei, Y., Hong, M., Wan, W., Du, A., Lei, J., Zhao, B., et al. (2008). Unusually long-lasting multiple penetration of interplanetary electric field to equatorial ionosphere under oscillating IMF Bz. *Geophysical Research Letters*, *35*(2), L02102. https://doi.org/10.1029/2007gl032305